ARTICLES

Direct Probe of Spectrally Narrowed Emission from π-Conjugated Polymers: The Elucidation of Mechanism for Spectral Line Narrowing

Sae Chae Jeoung,[†] Dae Hong Jeong,[‡] Taek Ahn,[§] Ja-Young Han,[§,||] Min-Sik Jang,[§,⊥] Hong-Ku Shim,[*,§] and Dongho Kim[*,‡]

Laser Metrology Laboratory, Korea Research Institute of Standards and Science, Taejon 305-600, Korea, Center for Ultrafast Optical Characteristics Control and Department of Chemistry, Yonsei University, Seoul 120-749, Korea, and Center for Advanced Functional Polymers, Department of Chemistry and School of Molecular Science (BK21), Korea Advanced Institute of Science and Technology, 373-1 Kusong-dong Yusong-Gu, Taejon 305-701, Korea

Received: October 10, 2001; In Final Form: May 10, 2002

Femtosecond time-resolved emission as well as transient absorption spectroscopy of π-conjugated polymeric thin film revealed an apparent induction time for the appearance of spectrally narrowed emission (SNE) in contrast with an instantaneous buildup of normal emission. These ultrafast intensity-dependent spectroscopic studies demonstrate that the origin of SNE phenomena in π-conjugated polymer is amplified spontaneous emission (ASE), which induces prompt and efficient depopulation of singlet excitons. Furthermore, comparison of temporal profiles of SNE, normal emission and stimulated emission reveals that the photoexcitations responsible for SNE processes are singlet excitons. The temporal profiles of SNE measured by changing excitation power density, illuminated spot size, and average π-conjugation length of polymer show that a build-up time plays an important role in generating intense SNE. These findings imply that pumping geometry, sample morphology, defect sites, as well as crystallinity are strongly correlated with ASE processes.

Introduction

π-Conjugated polymeric material has attracted much attention as a promising candidate for electrooptic devices, such as light-emitting diode (LED), photoconductor, and optical switches.[1,2] Furthermore, the realization of a new solid-state plastic laser has gained prospects after reports on lasing action in solution,[3−5] microcavity structures,[6−10] dip-coated optical fibers,[11] and distributed feedback geometry.[12] Recently a German research team has reported nearly diffraction-limited laser emission with a two-dimensional photonic band structure based on conjugated ladder-type poly(*p*-phenylene) polymer (LPPP) as the active layer.[13] In addition to lasing, there have been reports on the spectrally narrowed emission (SNE) from π-conjugated polymer films under high excitation densities as illustrated in Figure 1.[14−19] But the underlying mechanism for this peculiar phenomenon has been a subject of a great deal of controversy. The SNE in π-conjugated polymers has been explained in terms of amplified spontaneous emission (ASE) aided by waveguiding,[16−19] cooperative processes, such as superradiance or superfluorescence,[20−23] and the production of emissive biexcitons[24] or collective excitons.[25] Even though each of these propositions is supported by experimental evidence, it is now generally accepted that the SNE in polymer films is contributed by the ASE enhanced by the optical waveguiding in the films.

Most spectroscopic studies to elucidate the mechanism for SNE process have hitherto been focused on the time-resolved photoinduced absorption and stimulated emission (SE) measurements with varying the excitation power density.[14−25] On the bases of these measurements, SNE from π-conjugated polymers has been recently suggested to be a result of ASE and/or stimulated emission of incoherent excitations. More specifically, time-resolved transient absorption experiments exhibit a gradual decrease in the stimulated emission lifetime with increasing excitation density, which seems to be fairly consistent with a model utilizing ASE.

Nevertheless, the time-resolved measurement of SNE under various excitation densities is expected to provide direct evidences on the mechanism of the SNE process. Prior to our current work, there have been a few investigations[26−29] that reported the transient emission measurement of SNE by using fluorescence up-conversion technique. Among these, only one group[28,29] observed the induction time in the appearance of SNE which is a direct evidence of the build-up time for the ASE process. In the present study, we have tried to provide the direct spectroscopic evidences that the SNE of poly(*p*-phenylene vinylene) (PPV) derivatives shown in Figure 1 is contributed by the singlet excitons by using transient absorption as well as time-resolved emission measurements under the identical ex-

* To whom correspondence should be addressed. Hong-Ku Shim (e-mail: hkshim@sorak.kaist.ac.kr). Dongho Kim (e-mail: dongho@yonsei.ac.kr).
[†] Laser Metrology Laboratory.
[‡] Center for Ultrafast Optical Characteristics Control and Department of Chemistry.
[§] Center for Advanced Functional Polymers.
[||] Current address: Department of Chemistry and Biochemistry, University of California, Los Angeles, CA 90095-1569.
[⊥] Current address: SKC Co., Ltd. Central R&D Center, Suwon 440-840, Korea.

10.1021/jp013755g CCC: $22.00
Published on Web 08/08/2002

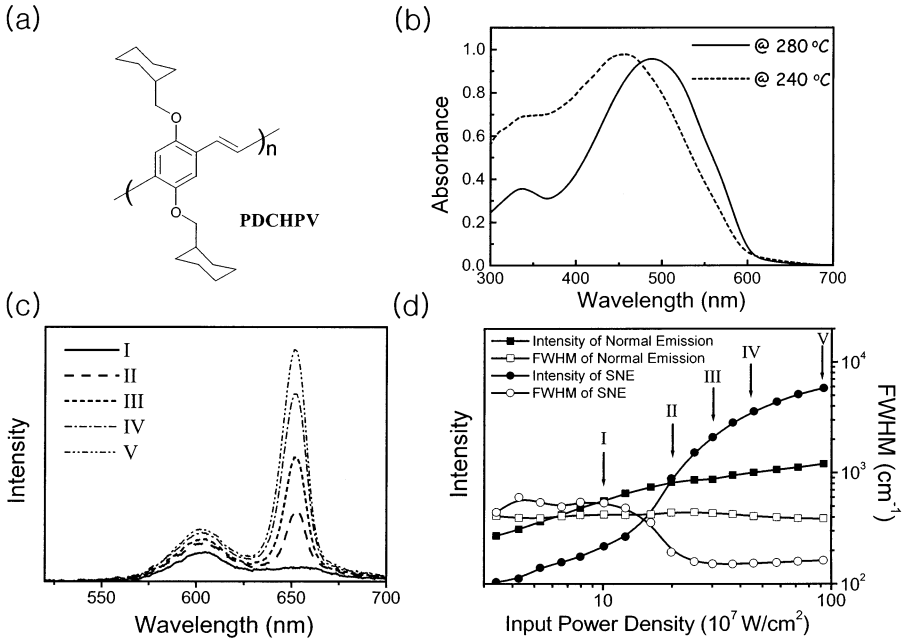

Figure 1. (a) Molecular structure and (b) UV−vis absorption spectrum of PDCHPV polymer film. (c) Time-integrated emission spectra of PDCHPV film upon photoexcitation at 400 nm with a pulse width of 150 fs at 1 kHz repetition rate. (d) The (■,●) intensities of the emission bands together with their fwhm at (□) 600 nm and at (○) 650 nm as a function of excitation power density. The excitation power conditions marked by capital Roman numbers were employed to measure the temporal profiles for SNE, stimulated emission, and normal emission.

perimental conditions. And we have directly compared our results with the previous ones by Lee et al.[28,29] to gain further insight into the build-up process of SNE in polymer films.

Experimental Section

π-Conjugated polymer investigated in this work is a PPV derivative, poly[2,5-bis(cyclohexylmethoxy)-1,4-phenylenevinylene] (PDCHPV) (Figure 1a).[30] The precursor polymer was spin-coated on a glass substrate from $CHCl_3$ solution and was subjected to thermal elimination in vacuo at 280 °C for 6 h to prepare fully conjugated polymer thin film. The film thickness was kept to be in the range of 200 to 250 nm. Differential scanning calorimetry (DSC) and Thermo-gravimetric analysis (TGA) reveal that the resultant film is highly stable up to 400 °C. The PDCHPV film shows a broad absorption at 465 nm and its band edge is ∼595 nm, as shown in Figure 1b. The emission intensity from this film was found to be constant up to 1 h under high excitation power density even in air, and up to 6 h under dried nitrogen atmospheric condition. We also found that the film shows high photochemical damage threshold for excitation power density compared with other PPV derivatives such as PPV and MEH−PPV (poly[2-methoxy-5-(2′-ethylhexyloxy)-1,4-phenylenevinylene]). These unique characteristics of the current π-conjugated polymer allow us to obtain a set of reliable spectroscopic data to provide direct evidences on the mechanism for SNE phenomena occurring in π-conjugated polymer film.

The detailed description of the femtosecond transient absorption setup employed in this work was given elsewhere.[31] Briefly, the excitation pulses at ∼400 nm were generated by frequency doubling of the amplified high-power Ti:sapphire laser output (800 nm, 120 fs at 1 kHz). The absorption change after photoexciation at ∼400 nm was probed by the delayed femotosecond white-light continuum pulses generated in water and was recorded by a spectrograph equipped with a charge-coupled device (CCD) detector. The absorption change was measured by the difference in optical densities between the presence and the absence of the pump pulses. The group delay dispersion by the white-light continuum was compensated for better time resolution. For time-resolved emission experiment, we employed fluorescence up-conversion technique based on the same amplified high-power femtosecond Ti:sapphire laser used for transient absorption measurements, which enables us to measure the emission decay profiles with ∼100 fs time resolution after deconvolution. Using this method, we were able to keep track of the evolution of time-resolved SNE spectra. The conjugated polymer was photoexcited at 400 nm, which is far from the absorption band edge to avoid any coherent artifact like stimulated Raman gain at the emission wavelength. The ultraviolet light, which results from sum frequency generation between emission from π-conjugated polymer and fundamental femtosecond optical pulses at 800 nm, was dispersed by monochromator with 0.5 nm spectral resolution and detected by a high-gain photomultiplier as well as a CCD detector. Both the emission wavelength and the delay time between pump and gate pulses were simultaneously controlled by a personal computer. The measured temporal profiles of well-known chromophores show that the full width at half-maximum (fwhm) of instrumental response function is ca. 250 fs at the emission wavelength of ∼600 nm.

Results

Figure 1c shows the time-integrated emission spectra with a change of excitation power density upon photoexcitation at 400 nm with 150 fs laser pulses focused loosely to a spot size of 1.5 mm in diameter. Under lower than 100 MW/cm^2 excitation power density, the emission spectrum with two bands at 600 and 650 nm exhibits the same fwhm of 450 cm^{-1} as those observed upon photoexcitation at 442 nm from a cw HeCd laser. An increase in the excitation power density, however, changes the overall emission spectral feature abruptly to SNE peaking at 650 nm with fwhm of 150 cm^{-1}, while maintaining the same fwhm of the band at 600 nm. The log−log plot in Figure 1d shows that the total emission intensity monotonically increases

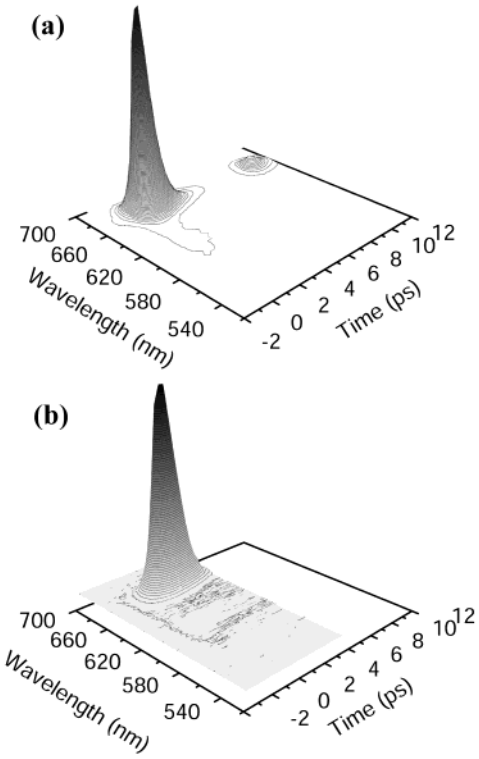

Figure 2. Three-dimensional plots of time-resolved emission spectra of PDCHPV film upon photoexcitation at 400 nm, where the spectra were measured by using a CCD detector with a step of 0.3 ps delay time. The polymer film was exposed to the pump power density of (a) 1 GW/cm^2 and (b) 100 MW/cm^2 with a spot size of 2 mm in diameter.

with an excitation power density up to 1 GW/cm^2, while both SNE and normal emission start to exhibit a nonlinear behavior above ~100 MW/cm^2.

We have constructed the time-resolved emission spectra of PDCHPV thin film under the excitation power density of 1 GW/cm^2, which is far above the onset value for the appearance of SNE. These results are displayed in a three-dimensional plot in Figure 2a. According to the time-integrated emission spectra (see Figure 1c), the two bands at 600 and 650 nm correspond to normal emission and SNE, respectively. The sharp and fast decaying (<2 ps) emission band at 650 nm dominates the overall emission spectrum. A distinct observation in the plot of Figure 2a is a train of events for SNE, which is separated by ~8.8 ps judging from peak-to-peak positions. This peculiar feature persists longer than 30 ps in delay time. This peak is thought to be caused by the front surface scattering of the SNE from the quartz plate with a thickness of 1.3 mm reflected from the other surface of the plate (1.3 mm $\times$ 2 $\times$ 3.3 ps/mm). The equal spacing of this time interval regardless of the excitation power density also supports this interpretation. We recorded the same spectra with decreasing the excitation power density to the level of onset value for SNE, which are displayed in Figure 2b in three-dimensional plot. The interesting finding is a time lag in the appearance of SNE in contrast with an instantaneous buildup of normal emission. Under this condition, the SNE reaches its maximum intensity at the delay time of about 2 ps after the initial appearance of normal emission, though only 0.5 ps time lag was observed in the appearance of SNE under high excitation power density as shown in Figure 2a. A further decrease of the excitation power density lower than the onset value for SNE results in a disappearance of SNE in the time-resolved emission spectra of PDCHPV film.

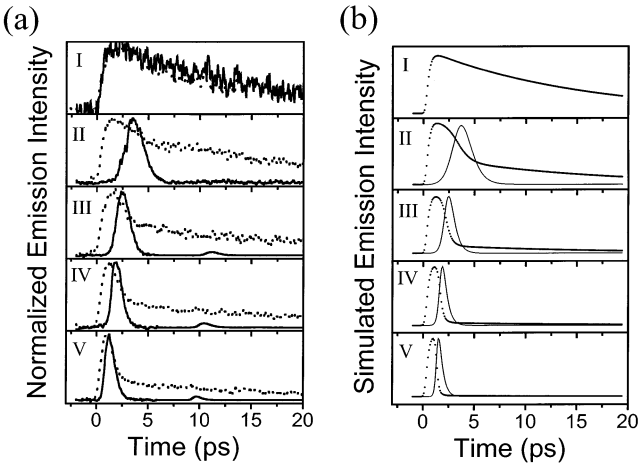

Figure 3. (a) Normalized temporal profiles of (· ·) normal emission and (—) SNE with the excitation power density marked in Figure 1d as I, II, III, IV, and V. (b) Simulated emission decay profiles based on the eqs 1−4 in the text. The stimulated emission cross section of $\sigma_{SE} \approx 10^{-16}$ cm^2 and $\kappa < \tau_c^{-1} = c/l_c \approx 3$ ps^{-1} by assuming the cooperative length, or l_c, to be 100 μm were taken. For each simulation N_o are chosen to be 1.4×10^4, 1.4×10^5, 1.68×10^5, 1.96×10^5, and 2.22×10^5 for the cases of I, II, III, IV, and V. The f value is adjusted to be 0.11 for optimum proximity of the simulated curves to the experimental curves. All parameters except N_o are the same for all the simulations.

Figure 3a presents the emission temporal profiles at 600 and 650 nm, which correspond to the maximum wavelengths for normal emission and SNE, respectively, under five different excitation densities as marked in Figure 1d. Under the excitation power density of lower than the onset value for SNE (Figure 3I), the temporal profile for normal emission at 600 nm exhibits nonexponential decay due to inhomogeneously broadened density of states with a time dependent distribution of hopping rates. The temporal profiles at 600 and 650 nm exhibit almost the same features indicating that the identical emissive species are involved under the used excitation power density. On the other hand, a slight increase above the onset value for SNE in the excitation power density changes the decay of SNE at 650 nm dramatically (Figure 3II). A further increase in the excitation power density up to ~1 GW/cm^2 affects significantly the decay profiles of both normal emission at 600 nm and SNE at 650 nm, leading to nonexponential decay. More importantly, a so-called "induction time", which is a time lag in the appearance of SNE after an instantaneous buildup of normal emission, was clearly observed in the temporal profiles of normal emission and SNE as shown in Figure 3II−V.[28,29] The induction time becomes shorter along with an increase in the excitation power density.

We also measured the chirp-free transient absorption decay to explore the dynamics of stimulated emission process under the same excitation power densities used to probe SNE phenomena. We could not observe any structural features of SE in the wavelength region of SNE by changing the illuminated spot size from 0.7 to 3 mm in diameter and the pump-power density from 100 MW/cm^2 to 1 GW/cm^2. Figure 4 shows the three-dimensional plot of time-resolved transient absorption spectra of PDCHPV film. It should be noted that there exists a time lag of ~200 fs between the stimulated emission at 650 nm and the ground-state bleaching below 550 nm. This time difference is believed to be due to the lattice relaxation processes of the initially prepared highly excited (vibrationally hot) excitons in the formation of Frenkel-type bound excitons. During this period, the spectral relaxation provided by the transfer of

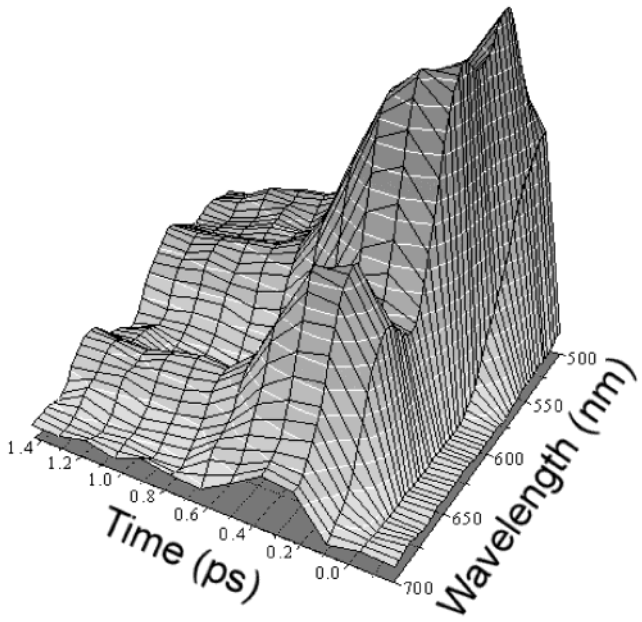

Figure 4. Three-dimensional plot of chirp-free time-resolved $\Delta T/T$ spectra of PDCHPV film. It should be noted that there exists a time-lag of ~200 fs between the stimulated emission at 650 nm and the ground-state bleaching below 550 nm.

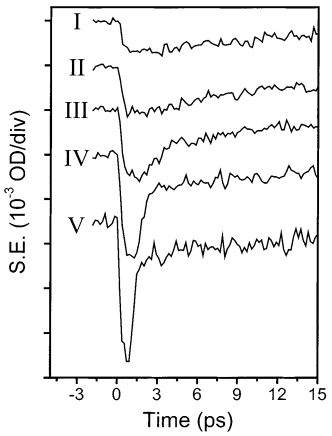

Figure 5. Normalized temporal profiles for stimulated emission ($\Delta T/T$) observed from femtosecond pump−probe experiment under five different excitation power densities, which are the same as those in Figure 3. The pump and probe wavelengths were 400 and 650 nm, respectively. By changing the probe intensity, we confirmed no contribution from photoinduced absorption at 650 nm.

excited states among the inhomogeneously broadened density of excitations has occurred simultaneously, because there is a statistical variation in the effective conjugation lengths and the random spatial distribution of the polymer segments. Figure 5 shows the typical power dependence of the stimulated emission dynamics at the illuminated spot size of about 2 mm under five different excitation densities as marked in Figure 1d at 650 nm, where the contribution from both ground-state bleaching and excited-state absorption is negligible. The overall stimulated emission decay profiles under various excitation densities (Figure 5) are quite similar to the normal photoluminescence decay profiles under the same excitation densities (dotted lines in Figure 3). This feature indicates that the same photoexcitations (singlet excitons) are responsible for the photoluminescence and stimulated emission decay processes, where two different methods were employed to distinguish photoluminescence and stimulated emission signals (fluorescence up-conversion and transient absorption).

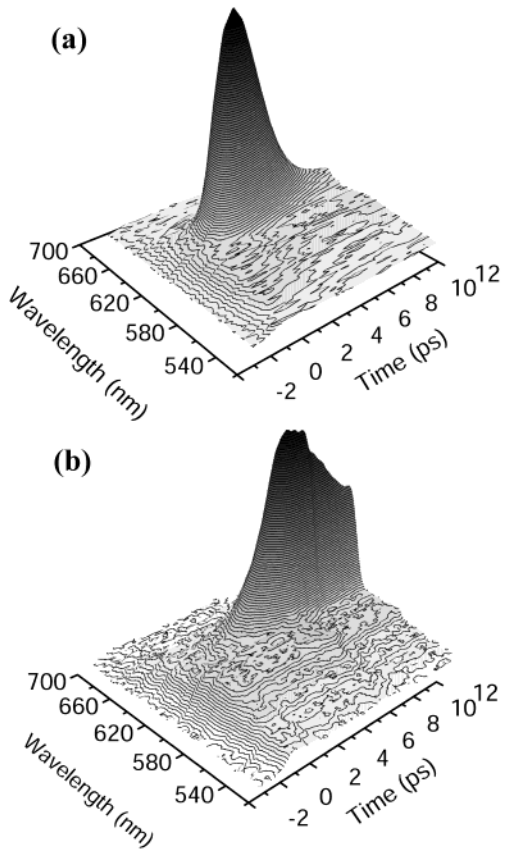

Figure 6. 3-dimensional plots of time-resolved emission spectra of PDCHPV film prepared at 240 °C. The excitation power density of (a) 1 GW/cm^2 and (b) 100 MW/cm^2 with a spot size of 2 mm in diameter was employed. The other experimental conditions are the same as those in Figure 2. It should be noted that the time-lag between normal emission at 580 nm and SNE at 630 nm is longer than (a) 3 ps and (b) 6 ps under this photoexcitation condition.

To gain insight into the relationship between the SNE process and the quality of polymer sample, we have carried out a series of similar experiments on the PDCHPV sample prepared at 240 °C, which gives rise to incomplete conjugation with a large inhomogeneity in conjugation length distributions. Figure 6a displays a three-dimensional plot of time-resolved emission spectra of PDCHPV film prepared at 240 °C under the photoexcitation density of 1 GW/cm^2, which is the same as that in Figure 2a. It is interesting to observe that the time-lag between normal emission at 580 nm and SNE at 630 nm is longer than 3 ps under this photoexcitation condition, which is much larger than that in the PDCHPV film prepared at 280 °C at the same excitation density (Figure 2a). It is to be noted that the emission from the PDCHPV film prepared at 240 °C is shifted to higher energy by ~20 nm with broadening due to shorter conjugation length and larger variation in its distribution than that prepared at 280 °C. The spectral and temporal features of normal emission appearing at higher energy side (~580 nm) show a clear ultrafast evolution of energy migration to lower energy sites (~630 nm) within the inhomogeneously broadened density of excited states because there is a large variation in conjugation length of π-conjugated polymers prepared at 240 °C.[32] Figure 6b shows a three-dimensional plot of time-resolved emission spectra of PDCHPV film prepared at 240 °C at the excitation power density of 100 MW/cm^2 which is the same as that in Figure 2b. The time lag between normal emission at 580 nm and SNE at 630 nm is longer than 6 ps under this photoexcitation condition,

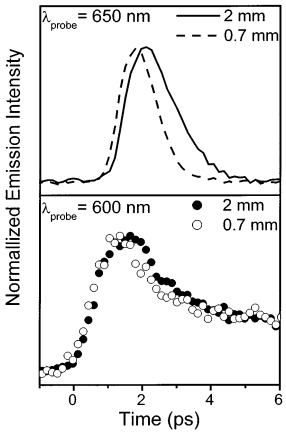

Figure 7. Normalized temporal profiles for (a) SNE and (b) normal emission at two different illuminated spot sizes of 0.7 mm and 2 mm in diameter. The excitation power density was kept the same.

which is also much larger than that observed in the PDCHPV film prepared at 280 °C at the same excitation density (Figure 2b).

If the SNE process is governed by the ASE process aided by the waveguiding effect, the light propagation time across the excited area should be important for the overall process.[33,34] To clarify this point, the SNE dynamics was measured by changing the illuminated spot size while maintaining the same photon density (Figure 7). The power density employed in this experiment was similar to that in Figure 3(III). As can be seen, there is a clear difference in the SNE dynamics at 650 nm depending on the illuminated area, but the temporal profiles of the normal emission at 600 nm are similar to each other (Figure 7). Not only the decay dynamics but the induction time becomes shorter in the case of small illuminated spot size. The ASE appears routinely in the stimulated emission of high gain media due to optical feedback via light scattering. This process was reported to be enhanced in the case of thin stripe excitation in proportion to the stripe length. Since this phenomena is caused by the backscattering occurring repeatedly along the entire length of the stripe excitation,[35] this process becomes sensitive to the arrangement of the scatters inside the excitation volume, implying that the morphology of the excited area as well as the illuminated area (geometry) is related to this process.[36,37]

Discussion

To gain further insight into the SNE process, it is appropriate to compare our current results with those by Lee et al.[28,29] because they reported the transient emission of thin films of 2,5-dioctyloxy PPV (DOO−PPV) at excitation density below and above the threshold density for SNE by using fluorescence up-conversion technique. In their measurements, a complex ASE buildup and decay dynamics as a function of excitation density and stripe length was observed. They also found that the exciton energy relaxation process within inhomogeneously broadened energy distribution becomes faster when ASE occurs. For high excitation intensity, they found that the spectral narrowing is accompanied by a lifetime reduction. And the delay in the SNE with respect to the photoluminescence onset depending on excitation intensity and illumination stripe length was also observed. More specifically, the transient emission of DOO−PPV measured with a round spot geometry at 630 nm corresponding to the SNE peak above the SNE threshold intensity shows the SNE in addition to normal photoluminescence. Also even with the highest excitation intensity (800 μJcm^{-2}/pulse) and the longest stripe length (500 μm) the transient emission exhibits relatively long-lived component persisting up to ∼15 ps in addition to the fast decaying component (∼2 ps). In our measurements, however, the temporal profiles of SNE processes only show fast decay component (1−2 ps) with a gradual shortening of the time delay in reaching the maximum SNE signal with an increase of the excitation intensity (solid lines in Figure 4). Lee et al.[28,29] also observed a second, delayed stimulated emission buildup which was explained by the fact that following the ultrafast decay caused by the SE in the film the MSCEX (the most strongly correlated excitons) states with superior radiative coupling are produced again due to the prolonged generation term. But actually this peculiar process does not seem to occur, because the temporal profiles they observed can be simply produced by a mixture of normal photoluminescence and SNE temporal profiles under a certain condition by changing the excitation intensity and stripe length (dotted and solid lines in Figure 4). Accordingly, the temporal profiles they observed are not due solely to SNE processes but to the mixture of SNE and normal photoluminescence which results in the second SE buildup, relatively long-lived component remaining up to ∼15 ps and complex forms of rise/decay curves. The temporal profiles of SNE processes monitored in the present work exhibit symmetric features with a gradual shortening of the delay time in reaching the maximum SNE signal and a concomitant shortening of rise and decay process with an increase in the excitation intensity without any long-lived components (solid lines in Figure 4). In our cases relatively slow rise and decay curves were observed even under high photoexcitation density in incompletely conjugated polymer films prepared at 240 °C. Thus, the morphologies of the polymer films seem to be strongly correlated with the SNE processes in addition to the excitation intensity and pumping geometry (stripe length). Overall, the most plausible explanation for the discrepancies between our measurements and the previous ones by Lee et al.[28,29] is that there is a difference in the spectral resolution for the fluorescence up-conversion and the morphologies of the polymer films.

It is relevant to consider the origin of the induction time as well as its excitation power dependence observed in this work. For a given position within the photoexcited area the rate equations can be set up for the population and photon density based on the previous works.[18,19] Here only a brief summary is given to provide a model for the decay dynamics of SNE. Since we observed an induction-time for a buildup of ASE process, we consider the density of initially prepared unrelaxed excitations N_2 responsible for normal emission and the density of relaxed excitations N_1 to give rise to ASE.

$$\frac{dN_2(t)}{dt} = (\tau_f^{-1} + \tau_i^{-1})N_2(t) \tag{1}$$

$$\frac{dN_1(t)}{dt} = \tau_i^{-1}N_2(t) - \tau_f^{-1}N_1(t) - c\int_0^o \sigma_{SE}N_1(t)q(\omega,t)d\omega \tag{2}$$

Here t_i is the relaxation time for the unrelaxed excitations prior to ASE process. τ_f is the fluorescence decay time for excitations. The third term in eq 2 represents the depletion of relaxed excitations via stimulated emission, and q is the photon density per unit frequency. In turn, the photon density change is given by the following equation:

$$\frac{dq(\omega,t)}{dt} = -\kappa q(\omega,t) + f\tau_f^{-1}\frac{1}{2\pi}gN_1(t) + c\sigma_{SE}N_1(t)q(\omega,t) \tag{3}$$

Here, κ indicates the propagation of photons in direction depending on pumping geometry,[19] and the second and third terms represent spontaneous and stimulated emission, respectively. The factor f considers the fraction of excitations that couple into waveguide modes, while g is the line shape function of the fluorescence spectrum. σ_{SE} represents the stimulated emission cross section and c is the speed of light. $N_2(t)$ becomes

$$N_2(t) = N_o \exp(-(\tau_f^{-1} + \tau_i^{-1})t) \quad (4)$$

Here N_o represents the initial population after pumping, which is proportional to the excitation power density. Considering the instrument response time (250 fs) the convoluted function of eq 4 was used. The stimulated emission cross section of $\sigma_{SE} \approx 10^{-16}$ cm^2 was taken. $\kappa < \tau_c^{-1} = c/l_c \approx 3$ ps^{-1} was given by assuming the cooperative length, or l_c, to be 100 μm.[38,39] For each simulation N_o are chosen to be $N_o = 1.4 \times 10^4$, 1.4×10^5, 1.68×10^5, 1.96×10^5, and 2.22×10^5 for cases of I, II, III, IV, and V. The f value is adjusted to be 0.11 for optimum proximity of the simulated curves to the experimental curves. All parameters except N_o are the same for all curve simulations. As shown in Figure 3, the simulated temporal profiles for the normal emission and ASE are in an excellent accordance with the experimental observations in that the buildup and decay times for ASE decrease as well as a decrease of the long-lived component in the normal emission decay as we increase the pump intensity.

The induction time for ASE is proportional to the duration time for the photons to propagate at the speed of light in the medium over the distance of the gain length. Near at the threshold value of excitation density, the order of gain medium length is nearly up to mm, leading to the induction time of a few picoseconds. Under higher excitation densities, the ASE does not require a long gain medium, which results in a shortening of the induction time. Just after the induction time, however, the excited-state population results in an enhancement of their decay rates, because the SNE in π-conjugated polymer thin film undergoes rapid decay aided by the ASE process.[26] Spontaneously emitted photons are waveguided in the polymer film and amplified by stimulated emission processes. ASE requires optical gain, where a population inversion is prerequisite. The high density of excited states is rapidly reduced by the stimulated emission process. As soon as the condition for the population inversion is terminated, the ASE process stops.

The observed induction time and depletion rates of excitations in polymeric thin films are believed to be strongly dependent on the samples such as film quality, thickness fluctuation, morphology,[40] and crystallinity,[41] in addition to the photoexcitation density. From a microscopic viewpoint, these properties seem to be closely correlated with the sample homogeneity determined by molecular orientations[42,43] and interchain distances,[44] because the unrelaxed excited states start to couple to each other to build up a large population density especially at high photoexcitation density. Furthermore, the previous investigation[33] reveals that microstructure of π-conjugated polymer film such as in-plain chain orientation, crystallinity, and structural coherence length is correlated with SNE phenomena. The most prominent feature is that in the disordered sample the gradual change from optical gain to induced absorption has occurred by increasing the pump energy. Thus, we can anticipate relatively well-ordered structures and hence good film quality of PDCHPV, which gives rise to significantly shorter build-up and depletion times as compared with the previous work.[28,29] In case of incompletely conjugated polymer films prepared at 240 °C, the induction time and depletion times of excitations become significantly larger at the same photoexcitation density as compared with the polymer film prepared at 280 °C. The larger inhomogeneity in the sample prepared at 240 °C evidenced by the broader and blue-shifted absorption spectrum indicates that the distribution in conjugation length becomes larger than that prepared at 280 °C. This results in longer induction time which is mainly contributed by the energy migration time in the formation of the relaxed excited states from the initially prepared unrelaxed ones. Simultaneously, the depopulation process of the high density of correlated exciton states is also retarded in case of inhomogeneous polymer films by the ASE processes because the ASE is dependent on the morphology of the polymer films.

Conclusion

The fluorescence up-conversion, transient absorption, beam-size dependence, different sample preparation temperatures and single pulse excitation experiments unequivocally demonstrate that the SNE phenomena in polymer films is the ASE process aided by waveguiding effect. An apparent induction time in the appearance of SNE was clearly observed with respect to the normal photoluminescence. The induction time and depopulation time were found to be dependent upon the illuminated spot size and excitation power density as well as the characteristics of polymer films. The observed SNE and related observations are not limited to the current PDCHPV; for example, other conjugated polymers, such as PPV, MEH−PPV (poly[2-methoxy-5-(2′-ethylhexyloxy)-1,4-phenylenevinylene]), and the blendings of MEH−PPV and DSiPV (poly[1,3-propane-dioxy-1,4-phenylene-1,2-ethylene(2,5-bis(tri-methylsilyl)1,4-phenylene)-1,2-ethylene-1,4-phenylene]) show the similar phenomena. The elucidation of mechanism for SNE phenomena provides prospects that spectrally narrowed organic π-conjugated polymeric light-emitting diodes based on charge injection may be fabricated by controlling its crystallinity and active size.

Acknowledgment. This work has been financially supported by National Creative Research Initiatives Program of the Ministry of Science and Technology of Korea (D.K.) and partially by Center for Advanced Functional Polymers (H.K.S.).

Supporting Information Available: Syntheses of PDCHPV and its precursors along with characterizations of PDCHPV. This material is available free of charge via the Internet at http://pubs.acs.org.

References and Notes

(1) Burrougher, J. H.; Bradley, D. D. C.; Brown, A. R.; Marks, R. N.; Mackay, K.; Friend, R. H.; Burn, P. L.; Holmes, A. B. *Nature* **1990**, *347*, 539.

(2) Bradley, D. D. C. *Curr. Opin. Solid State Mater. Sci.* **1996**, 1.

(3) Moses, D. *Appl. Phys. Lett.* **1992**, *60*, 3215.

(4) Brouwer, H. J.; Kransikov, V. V.; Hilberer, A.; Wildeman, J.; Hadziioznnou, G. *Appl. Phys. Lett*. **1995**, *66*, 3404.

(5) Holzer, W.; Penzkofer, A.; Gong, S.-H.; Bleyer, A.; Bradley, D. D. C. *Adv. Mater*. **1996**, *8*, 974.

(6) Tessler, N.; Denton, G. H.; Friend, R. H. *Nature* **1996**, *382*, 695.

(7) Díaz-García, M. A.; Hide, F.; Schwartz, B. J.; McGehee, M. D.; Andersson, M. R.; Heeger, A. J. *Appl. Phys. Lett*. **1997**, *70*, 3191.

(8) Zenz, C.; Graupner, W.; Tasch, S.; Leising, G.; Müllen, K.; Scherf, U. *Appl. Phys. Lett.* **1997**, *71*, 2566.

(9) Virgili, T.; Lidzey, D. G.; Bradley, D. D. C.; Cerullo, G.; Stagira, S.; De Silvestri, S. *Appl. Phys. Lett.* **1999**, *74*, 2767.

(10) Leising, G.; Tasch, S.; Brandstätter, C.; Graupner, W.; Hampel, S.; List, E. J. W.; Meghdadi, F.; Zenz, C.; Schlichting, P.; Rohr, U.; Geerts, Y.; Scherf, U.; Müllen, K. *Synth. Met.* **1997**, *91*, 41.

(11) Frolov, S. V.; Shkunov, M.; Vardeny, Z. V.; Yoshino, K. *Phys. Rev. B* **1997**, *56R*, 4363.

(12) Riechel, S.; Lemmer, U.; Feldmann, J.; Benstem, T.; Kowalsky, W.; Scherf, U.; Gombert, A.; Wittwer, V. *Appl. Phys. B* **2000**, *71*, 897.
(13) Riechel, S.; Kallinger, C.; Lemmer, U.; Feldmann, J.; Gombert, A.; Wittwer, V.; Scherf, U. *Appl. Phys. Lett.* **2000**, *77*, 2310.
(14) Hide, F.; Schwartz, B. J.; Díaz-García, M. A.; Heeger, A. J. *Science* **1996**, *273*, 1833.
(15) McGhee, M. D.; Heeger, A. J. *Adv. Mater*. **2000**, *12*, 1566.
(16) Denton, G. J.; Tessler, N.; Stevens, M. A.; Friend, R. H. *Adv. Mater.* **1997**, *9*, 547.
(17) Haugeneder, A.; Hilmer, M.; Kallinger, C.; Perner, M.; Spirkl, W.; Lemmer, U.; Feldman, J.; Scherf, U. *Appl. Phys. B*: *Laser Opt*. **1998**, *66*, 389.
(18) Doan, V.; Tran, V.; Schwartz, B. J. *Chem. Phys. Lett.* **1998**, *288*, 576.
(19) Haugeneder, A.; Neges, M.; Kallinger, C.; Spirkl, W.; Lemmer, U.; Feldmann, J.; Amann, M.-C.; Scherf, U. *J. Appl. Phys.* **1999**, *85*, 1124.
(20) Long, X.; Malinowski, A.; Bradley, D. D. C.; Inbeasekaran, M.; Woo, E. P. *Chem. Phys. Lett*. **1997**, *272*, 6.
(21) Frolov, S. V.; Gellermann, W.; Ozaki, M.; Yoshino, K.; Vardeny, Z. V. *Phys. Rev. Lett*. **1997**, *78*, 729.
(22) Frolov, S. V.; Ozaki, M.; Gellermann, W.; Vardeny, Z. V.; Yoshino, K. *Jpn. J. Appl. Phys.* **1996**, *35*, L1371.
(23) Jeoung, S. C.; Kim, Y. H.; Kim, D.; Han, J.-Y.; Jang, M.-S.; Shim, H.-K. *Appl. Phys. Lett*. **1999**, *74*, 212.
(24) Kranzelbinder, G.; Nisoli, M.; Stagira, S.; De Silvestri, S.; Lanzani, G.; Müllen, K.; Scherf, U.; Graupner, W.; Leising, G. *Appl. Phys. Lett*. **1997**, *71*, 2725.
(25) Gelinck, G. H.; Warman, J. M.; Remmers, M.; Neher, D. *Chem. Phys. Lett*. **1997**, *265*, 320.
(26) Wegmann, G.; Schweitzer, B.; Hertel, D.; Giessen, H.; Oestreich, M.; Scherf, U.; Müllen, K.; Mahrt, R. F. *Chem. Phys. Lett.* **1999**, *312*, 376.
(27) Nisoli, M.; Stagira, S.; Zavelani-Rossi, M.; De Silvestri, S.; Mataloni, P.; Zens, C. *Phys. Rev. B* **1999**, *59*, 11328.
(28) Lee, C. W.; Wong, K. S.; Huang, J. D.; Frolov, S. V.; Vardeny, Z. V. *Chem. Phys. Lett.* **1999**, *314*, 564.
(29) Lee, C. W.; Wong, K. S.; Huang, J. D.; Frolov, S. V.; Vardeny, Z. V. *Synth. Met.* **2001**, *116*, 61.
(30) Jang, M. S. et al. Submitted for publication.
(31) Cho, H. S.; Yang, S. I.; Kim, S. K.; Shin, E.-j.; Kim, D. *J. Phys. Chem. B* **1999**, *103*, 6504.
(32) Kersting, R.; Lemmer, U.; Mahrt, R. F.; Leo, K.; Kurz, H. Bässler, H.; Göbel, E. O. *Phys. Rev. Lett.* **1993**, *70*, 3820.
(33) Pham, T.-A.; Barisien, T.; Grayer, V.; Guidoni, L.; Hadziioannou, G.; Bijot, J.-Y. *Chem. Phys. Lett.* **2000**, *318*, 459.
(34) Pham, T.-A.; Daunois, A.; Merle, J. C.; Moigne, J. Le; Bigot, J.-Y. *Phys. Rev. Lett.* **1995**, *74*, 904.
(35) Frolov, S. V.; Shkunov, M.; Fujii, A.; Yoshino, K.; Vardeny Z. V. *IEEE J. Quantum Electron*. **2000**, *36*, 2.
(36) Hide, F.; Díaz-García, M. A.; Schwartz, B. J.; Andersson, M. R.; Pei, Q.; Heeger, A. J. *Chem. Phys. Lett*. **1996**, *256*, 424.
(37) McGhee, M. D.; Gupta, R.; Veenstra, S.; Miller, E. K.; Díaz-García, M. A.; Heeger, A. J. *Phys. Rev. B* **1998**, *58*, 7035
(38) Frolov, S. V.; Vardeny, Z. V.; Yoshino, K. *Phys. Rev. B* **1998**, *57*, 9141.
(39) Arecchi, F. T.; Courtens, E. *Phys. Rev. A* **1970**, *2*, 1730.
(40) Silva, C.; Russell, D. M.; Stevens, M. A.; Mackenzie, J. D.; Setayesh, S.; Müllen, K.; Friend, R. H. *Chem. Phys. Lett.* **2000**, *319*, 494.
(41) Yang, C. Y.; Hide, F.; Díaz-García, M. A.; Heeger, A. J.; Cao, Y. *Polymer* **1998**, *39*, 2299.
(42) van Hutten, P. F.; Wildeman, J.; Meetsma, A.; Hadziioannou, G. *J. Am. Chem. Soc.* **1999**, *121*, 5910.
(43) Claes, L.; François, J.-P.; Deleuze, M. S. *Chem. Phys. Lett.* **2001**, *339*, 216.
(44) Cornil, J.; Heeger, A. J.; Bredas, J. L. *Chem. Phys. Lett.* **1997**, *272*, 463.